3D Printing of Ionic Conductors for High-Sensitivity Wearable Sensors

Xiangyu Yin, Yue Zhang, Xiaobing Cai, Qiuquan Guo, Jun Yang* Zhong Lin Wang

Table of contents

The supplementary information file includes 1 supplementary note, 7 supplementary Figures (Figures S1-S7), 3 supplementary Tables (Table S1-S3) and 1 supplementary video (Video S1).

Supplementary Note

Modelling of capacitive sensors. For a sensor using plat hydrogel film as electrodes, the overall capacitance (C) is determined by the overlapped area of two hydrogel electrodes (*A*) and the thickness of the VHB dielectric layer (d_0),

$$C = \varepsilon_0 \varepsilon_1 \frac{A}{d_0} \quad (1)$$

where, ε_0 is the dielectric constant of vacuum (ε_0= 8.85^{-12} F m^{-1}), ε_1 is the relative dielectric constant for the dielectric layer and its value is 4.7 for the VHB tape[1]. The initial thickness of the VHB dielectric layer d_0 is 500 µm. Stretching or pressing the sensor will decrease the thickness of the dielectric layer d_0 and increase the overlapped area of the two hydrogel electrodes, consequently causing an increase in capacitance.

For structured sensor, each unit cell of the device is defined by four types of areal components, a real overlapping area A_{re}×4, an upper-suspended area A_{up}×2 (air gap located between top electrode and VHB dielectric layer), a lower-suspended area A_{low}×2 (air gap located between bottom electrode and VHB dielectric layer), and a fully suspended area A_{sus}, as shown in Fig. 3c.

$$A_{unit} = 4A_{re} + 2A_{up} + 2A_{low} + A_{sus} \quad (1)$$

Therefore, the total capacitance of a unit cell (C_{unit}) in an array is composed of four types, a real overlapping capacitance C_{re}×4, a upper-suspended capacitance C_{up}×2, a lower-suspended capacitance C_{low}×2 and a fully suspended capacitance C_{sus}. It is descripted as equation (2).

$$C_{unit} = 4C_{re} + 2C_{up} + 2C_{low} + C_{sus} \quad (2)$$

where C_{re} is the capacitance of the dielectric between two hydrogel electrodes given by

$$C_{re} = \varepsilon_0 \varepsilon_1 \frac{A_{re}}{d_0} \quad (3)$$

C_{up} is the capacitance of the upper-suspended portion given by

$$\frac{1}{C_{up}} = \frac{1}{C_{d0}} + \frac{1}{C_{gap-up}} \quad (4)$$

where, C_{d0} is the capacitance of the dielectric layer at the upper-suspended portion given by

$$C_{d_0} = \varepsilon_0 \varepsilon_1 \frac{A_{up}}{d_0} \quad (5)$$

and $C_{gap\text{-}up}$ is the capacitance of the air gap at the upper-suspended portion given by

$$C_{gap-up} = \varepsilon_0 \frac{A_{up}}{d_1} \quad (6)$$

where d_1 is the thickness of air gap, and in this work, its initial value is 200 µm. Substituting (5) and (6) into (4), we obtain:

$$C_{up} = \varepsilon_0\varepsilon_1\frac{A_{up}}{d_0 + \varepsilon_1 d_1} \quad (7)$$

Similarly, the capacitance of the lower-suspended portion can be given by

$$C_{low} = \varepsilon_0\varepsilon_1\frac{A_{low}}{d_0 + \varepsilon_1 d_2} \quad (8)$$

where, d_2 is the thickness of air gap at the lower-suspended portion.
And C_{sus} is the capacitance of the fully suspended portion given by

$$\frac{1}{C_{sus}} = \frac{1}{C'_{d_0}} + \frac{1}{C'_{gap-up}} + \frac{1}{C'_{gap-low}} \quad (9)$$

where C'_{d_0} is the capacitance of the dielectric layer between two air gaps given by

$$C'_{d_0} = \varepsilon_0\varepsilon_1\frac{A_{sus}}{d_0} \quad (10)$$

And C'_{gap-up} and $C'_{gap-low}$ are the capacitances of the air gap located below and above the VHB dielectric layer at the fully suspended portion, respectively. They can be given by equations (11) and (12).

$$C'_{gap-up} = \varepsilon_0\frac{A_{sus}}{d_1} \quad (11)$$

$$C'_{gap-low} = \varepsilon_0\frac{A_{sus}}{d_2} \quad (12)$$

Substituting (10-12) into (9), we obtain:

$$C_{sus} = \varepsilon_0\varepsilon_1\frac{A_{sus}}{d_0 + \varepsilon_1 d_1 + \varepsilon_1 d_2} \quad (13)$$

Hence, the capacitance of an entire device with *n* sensing units is thus given by

$$C = nC_{unit} = n\varepsilon_0\varepsilon_1(\frac{4A_{re}}{d_0} + \frac{2A_{up}}{d_0 + \varepsilon_1 d_1} + \frac{2A_{low}}{d_0 + \varepsilon_1 d_2} + \frac{A_{sus}}{d_0 + \varepsilon_1 d_1 + \varepsilon_1 d_2}) \times 10^3 \quad (14)$$

Hence, for a sensor with the structural hydrogel films as electrodes, (the hydrogel film is structured with multi-parallel lines, and each line width and height is 200 μm), and 500-μm-thick VHB tape and air as the dielectric layer, the initial overall capacitance (C) can be expressed as follows equation (15).

$$C = nC^0_{unit} = n\varepsilon_0(8A_{re} + 1.39A_{up} + 1.39A_{low} + 0.42A_{su}) \quad (15)$$

For structured sensor-1, a 1 cm^2 square device is composed of 25×25 sensing units (*n*=625), and every sensing unit is divided into four areal components of A_{re}=1×10^{-8} m^2, A_{up}=2×10^{-8} m^2, A_{low}=2×10^{-8} m^2, A_{sus}= 4×10^{-8} m^2. Accordingly, its initial capacitance is calculated to be 3.96 pF, smaller than the predication for the planar sensor (8.31 pF). When the line-to-line spacing is 400 μm, a 1 cm^2 square sensor consists of 16×16 sensing units (n=256), and in each unit, A_{re}=1×10^{-8} m^2, A_{up}=4×10^{-8} m^2, A_{low}=4×10^{-8} m^2, and A_{sus}= 16×10^{-8} m^2. The initial capacitance for this sensor (structured sensor-2) is calculated to be 2.75 pF.

When applying an external force to the sensors in horizontal or orthogonal directions, all four types of areal components will undoubtedly increase, and the thickness of dielectric layer, d_0 and air gaps, d_1 and d_2 will reduce to varying degrees, thus resulting in an increase in capacitance according to equation (14). Therefore, by monitoring the changes of capacitance C of the sensors, strain and pressure can be detected.

Supplementary Figures

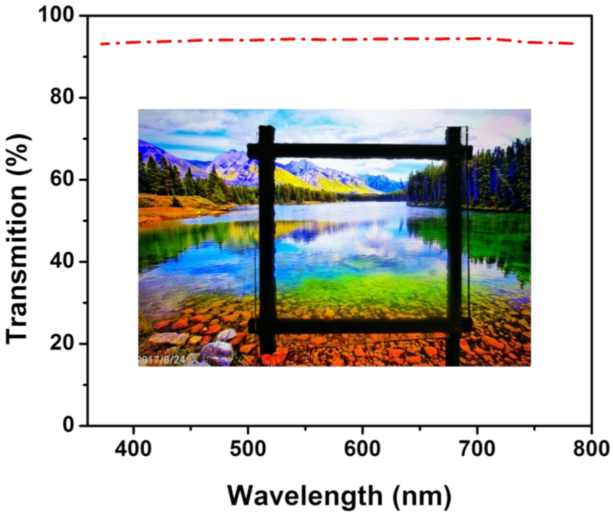

Supplementary Fig. 1 Light transmittance of PAAm-PEGDA-280 in the visible region.

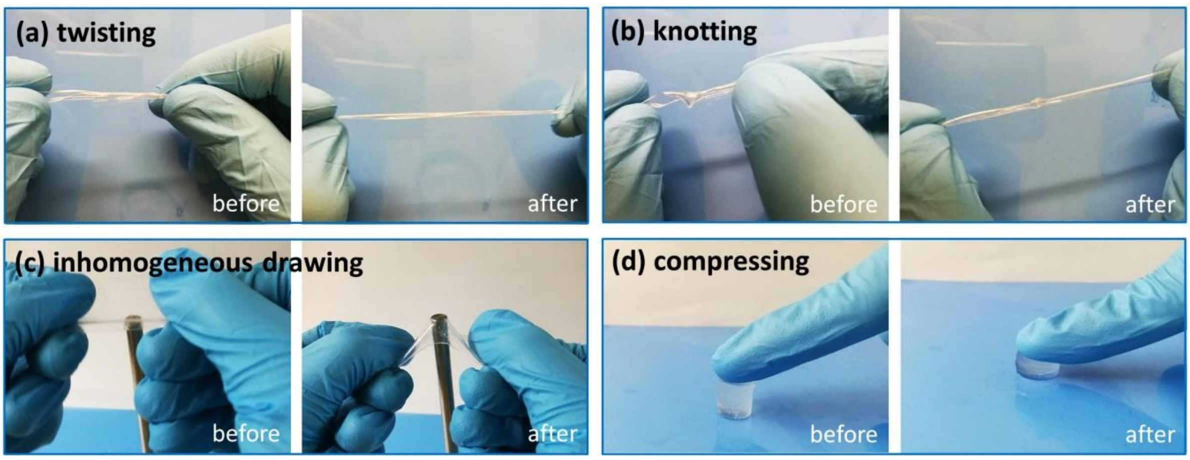

Supplementary Fig. 2 Mechanical deformation of PAAm-PEGDA-280 hydrogel. The hydrogel is capable of withstanding mechanical deformations: twisted (**a**) and knotted (**b**) stretching, inhomogeneous drawing (**c**) and compressing (**d**).

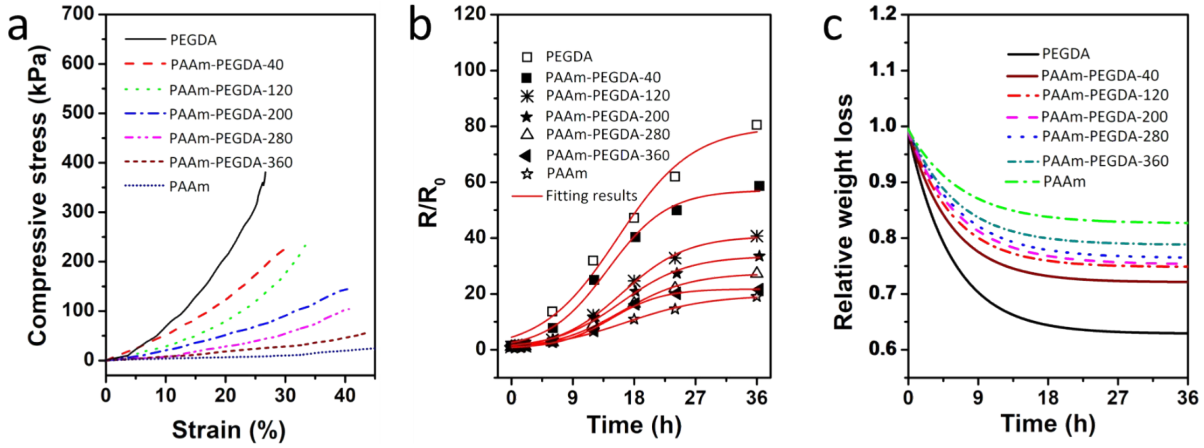

Supplementary Fig. 3 Mechanical and time-dependent properties. **a** Compressive strain-stress curves for hydrogels with different molecular compositions. Time dependences of **b** resistance change and **c** water retention for hydrogels with different molecular compositions.

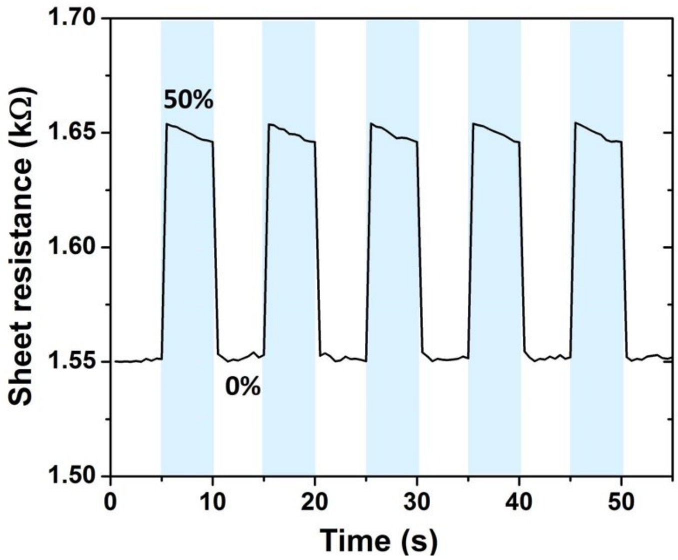

Supplementary Fig. 4 Representative resistance change of the PAAm-PEGDA-280 hydrogel film during stretching/releasing cycles of strain from 0 to 50%.

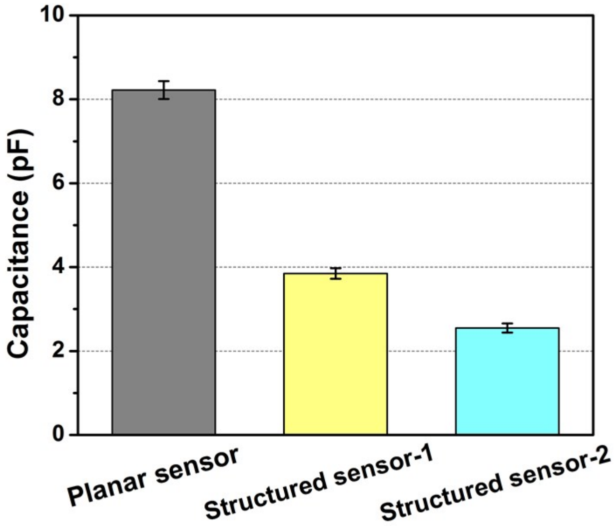

Supplementary Fig. 5 Measured initial capacitance for planar sensor, structured sensor-1 and structured sensor-2.

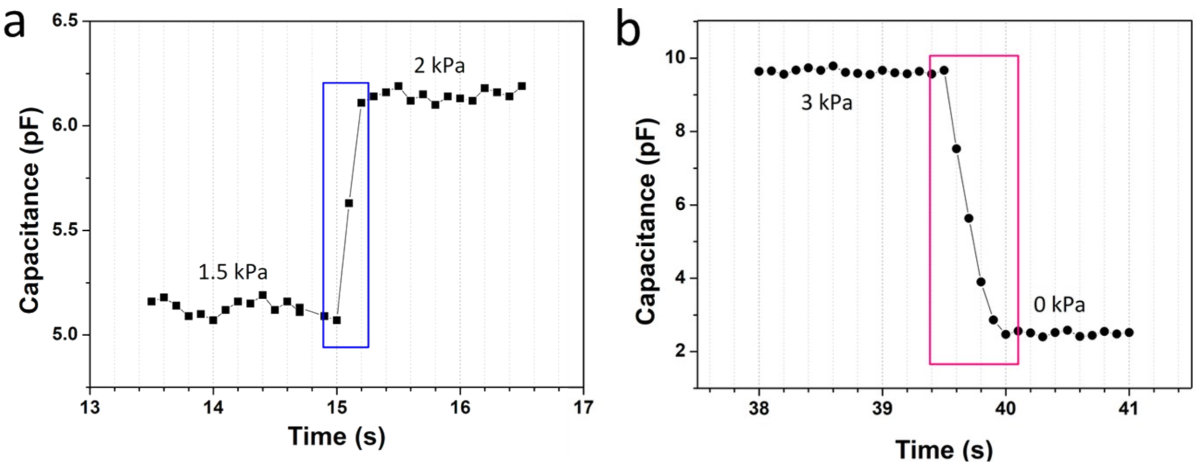

Supplementary Fig. 6 Response and relaxation time of the structured sensor-2 to application and release of external pressure loads. **a** Response time to increased pressure is about 200 ms. **b** Relaxation time to decreased pressure is about 500 ms

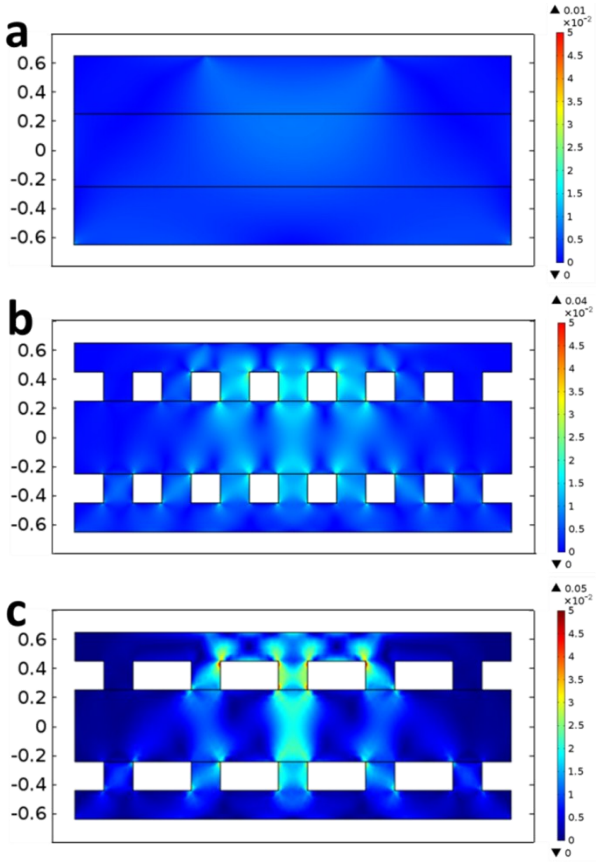

Supplementary Fig. 7 Strain distribution for three kinds of sensors when bearing a pressure load of 2 kPa. (**a**) planar sensor, (**b**) structured sensor-1 and (**c**) structured sensor-2.

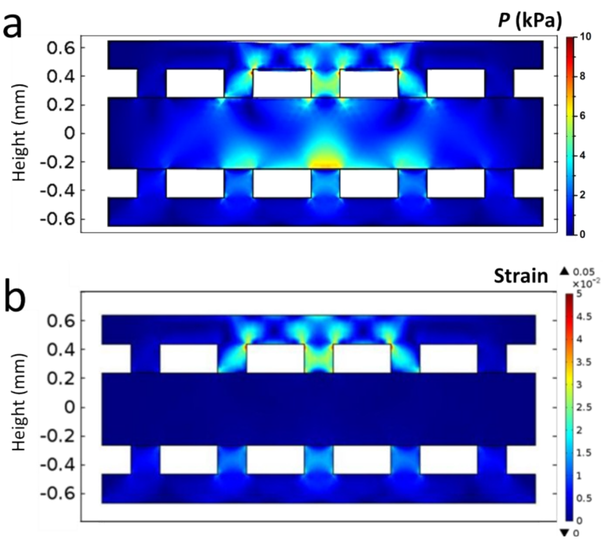

Supplementary Fig. 8 2D finite element simulations. **a** Von Mises stress and (**b**) strain distribution for hydrogel/PDMS/hydrogel when bearing a pressure load of 2 kPa.

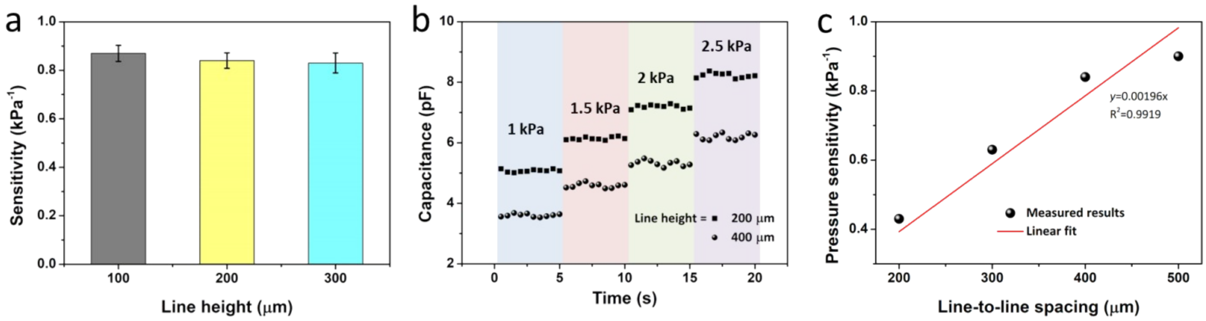

Supplementary Fig. 9 (a) Pressure sensitivity of the hydrogel sensors with different line heights. (b) Plots of capacitance response as a function of time for different applied pressures. (c) The linear relationship between pressure sensitivity of the structured sensors with line-to-line spacing.

Supplementary Tables

Table 1. Optimized parameters for the printing of PAAm-PEGDA hydrogels using an Asiga Pico 2 printer.

Build parameter	**Value**
Slice thickness	0.025 mm
Burn-in layers	1 layer
Slides per layer	1
Burn-in exposure time	2.2 s
Exposure time	2.2 s
Led wavelength	405 nm
Pixel size	39 µm

Table 2. Main compositions of the formulations for ionically conductive hydrogels.

Hydrogels	**Main compositions concentration (mol L^{-1})**			**C_{AAm}:C_{PEGDA} (molar ratio)**	**$\frac{m_{MgCl_2 + H_2O}}{m_{total}}$ (%)**
	AAm	**PEGDA**	**Mg^{2+}**		
PEGDA	0	0.1	2	—	66.7
PAAm-PEGDA-40	2.0	0.05	2	40:1	70.7
PAAm-PEGDA-120	3.0	0.025	2	120:1	72.7
PAAm-PEGDA-200	3.3	0.017	2	200:1	73.4
PAAm-PEGDA-280	3.5	0.0125	2	280:1	73.7
PAAm-PEGDA-360	3.6	0.01	2	360:1	73.9
PAAm	4.0	0	2	—	74.7

Table 3. Comparison of pressure sensors in previous reports.

Electrode	**Dielectric layer**	**Sensitivity** (kPa^{-1})	**Referenc e**
ACC/PAA/alginate hydrogel	VHB tape	0.17	2
PAAm hydrogel	VHB tape	0.1	3
ITO/PET	PDMS film	0.02 (unstructured) 0.55 (pyramid structured)	4
Ag NW	Ecoflex	1.62×10^{-3}	5
ITO/PET	Porous PDMS	0.26 kPa^{-1}, 0–0.33 kPa 0.01 kPa^{-1}, 0.33–250 kPa 0.9 $\times10^{-3}$ kPa^{-1}, 250–1 MPa	6
CNT	Ecoflex	0.59	7
SBS/Ag NPs	Kevlar fiber	0.21	8
Conductive Fabrics	microporous silicone	1.21×10^{-2}	9
Graphene	PDMS/SU8/Air	6.55×10^{-2}	10
Graphene	Porous Nylon	0.33	11
Graphene	GO foam	0.8 kPa^{-1}, 0–1.0 kPa 0.15 kPa^{-1}, 1.0–4.0 kPa	12
PEDOT:PSS	PDMS/Silica bead (500 nm)	1.0	13
Grid-structured hydrogel	PE	0.45	14
Ionogel	PDMS	0.43	15
ITO/PET	Porous PDMS	0.63	16
Graphite	PDMS	0.62	17
AgNWs	Microstructured ionic gel	54.3 kPa^{-1}, 0–0.5 kPa	18
Nafion	Air	5 nF kPa^{-1}, 0–5 kPa 0.15 nF kPa^{-1}, 10–30 kPa	19
Ag	Ecoflex	1.45×10^{-3}	20
AgNWs-healable PU	Graphene-healable PU	1.9	21

Line-structured hydrogel	VHB	0.84 kPa^{-1}	This work
3D-mesh hydrogel	VHB	0.91 kPa^{-1}	This work

Reference：

1. C. H. Yang, S. Zhou, S. Shian, D. R. Clarke and Z. G. Suo, *Materials Horizons*, 2017, **4**, 1102-1109.
2. Z. Lei, Q. Wang, S. Sun, W. Zhu and P. Wu, *Adv. Mater.*, 2017, **29**, 1700321.
3. J. Y. Sun, C. Keplinger, G. M. Whitesides and Z. Suo, *Adv. Mater.*, 2014, **26**, 7608-7614.
4. S. C. Mannsfeld, B. C. Tee, R. M. Stoltenberg, C. V. Chen, S. Barman, B. V. Muir, A. N. Sokolov, C. Reese and Z. Bao, *Nat Mater*, 2010, **9**, 859-864.
5. S. Yao and Y. Zhu, *Nanoscale*, 2014, **6**, 2345-2352.
6. S. Chen, B. Zhuo and X. Guo, *ACS Applied Materials & Interfaces*, 2016, **8**, 20364-20370.
7. X. Wang, T. Li, J. Adams and J. Yang, *Journal of Materials Chemistry A*, 2013, **1**, 3580-3586.
8. J. Lee, H. Kwon, J. Seo, S. Shin, J. H. Koo, C. Pang, S. Son, J. H. Kim, Y. H. Jang, D. E. Kim and T. Lee, *Adv. Mater.*, 2015, **27**, 2433-2439.
9. O. Atalay, A. Atalay, J. Gafford and C. Walsh, *Advanced Materials Technologies*, 2018, **3**, 1700237.
10. S. Pyo, J. Choi and J. Kim, *Adv Electron Mater*, 2018, **4**, 1700427.
11. Z. He, W. Chen, B. Liang, C. Liu, L. Yang, D. Lu, Z. Mo, H. Zhu, Z. Tang and X. Gui, *ACS Appl Mater Interfaces*, 2018, **10**, 12816-12823.
12. S. Wan, H. Bi, Y. Zhou, X. Xie, S. Su, K. Yin and L. Sun, *Carbon*, 2017, **114**, 209-216.
13. H. Kim, G. Kim, T. Kim, S. Lee, D. Kang, M. S. Hwang, Y. Chae, S. Kang, H. Lee, H. G. Park and W. Shim, *Small*, 2018, **14**, 1703432.
14. Z. Y. Lei, Q. K. Wang and P. Y. Wu, *Materials Horizons*, 2017, **4**, 694-700.
15. M. F. Lin, J. Q. Xiong, J. X. Wang, K. Parida and P. S. Lee, *Nano Energy*, 2018, **44**, 248-255.
16. S. Kang, J. Lee, S. Lee, S. Kim, J. K. Kim, H. Algadi, S. Al‐Sayari, D. E. Kim, D. Kim and T. Lee, *Adv Electron Mater*, 2016, **2**, 1600356.
17. K. Lee, J. Lee, G. Kim, Y. Kim, S. Kang, S. Cho, S. Kim, J. K. Kim, W. Lee, D. E. Kim, S. Kang, D. Kim, T. Lee and W. Shim, *Small*, 2017, **13**.
18. Z. Qiu, Y. Wan, W. Zhou, J. Yang, J. Yang, J. Huang, J. Zhang, Q. Liu, S. Huang, N. Bai, Z. Wu, W. Hong, H. Wang and C. F. Guo, *Adv. Funct. Mater.*, 2018, **28**.
19. Z. Zhu, R. Li and T. Pan, *Adv. Mater.*, 2018, **30**.
20. X. Zhao, Q. Hua, R. Yu, Y. Zhang and C. Pan, *Adv Electron Mater*, 2015, **1**, 1500142.
21. F. Liu, F. Han, L. Ling, J. Li, S. Zhao, T. Zhao, X. Liang, D. Zhu, G. Zhang, R. Sun, D. Ho and C.-P. Wong, *Chemistry – A European Journal*, 2018, **24**, 16823-16832.